Article

Energetically Driven Reorganization of a Modified Catalytic Surface under Reaction Conditions

Andrea Locatelli, Carlo Sbraccia, Stefan Heun, Stefano Baroni, and Maya Kiskinova

J. Am. Chem. Soc., **2005**, 127 (7), 2351-2357• DOI: 10.1021/ja045285k • Publication Date (Web): 29 January 2005

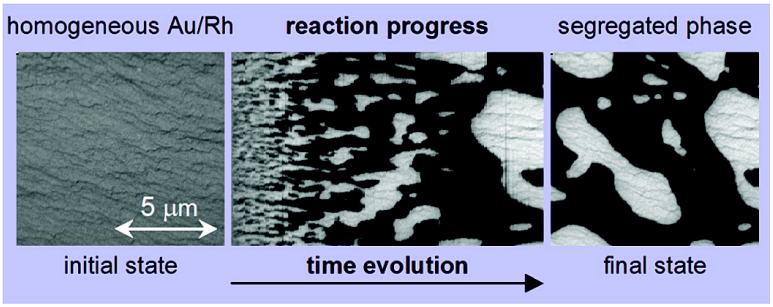

More About This Article

Additional resources and features associated with this article are available within the HTML version:

- Supporting Information
- Links to the 2 articles that cite this article, as of the time of this article download
- Access to high resolution figures
- Links to articles and content related to this article
- Copyright permission to reproduce figures and/or text from this article

View the Full Text HTML

J|A|C|S
ARTICLES
Published on Web 01/29/2005

Energetically Driven Reorganization of a Modified Catalytic Surface under Reaction Conditions

Andrea Locatelli,*,† Carlo Sbraccia,‡,§ Stefan Heun,|| Stefano Baroni,‡ and Maya Kiskinova†

Contribution from the Sincrotrone Trieste S.C.p.A., S.S. 14, km 163.5 in Area Science Park, 34012 Basovizza, Trieste, Italy, SISSA—Scuola Internazionale Superiore di Studi Avanzati and INFM DEMOCRITOS National Simulation Center, via Beirut 2-4, 34014 Trieste, Italy, Dipartimento di Fisica 'G.Galilei', Università di Padova, via Marzolo 8, I-35131 Padova, Italy, and Laboratorio Nazionale TASC, S.S. 14, km 163.5, Area Science Park, 34012 Basovizza, Trieste, Italy.

Received August 4, 2004; E-mail: andrea.locatelli@elettra.trieste.it

Abstract: The compositional and structural rearrangements at the catalyst surface during chemical reactions are issues of great importance for understanding and modeling the catalytic processes. Low-energy electron microscopy and photoelectron spectromicroscopy studies of the real-space structure and composition of a Au-modified Rh(110) surface during water formation reveal reorganization processes due to Au mass transport triggered by the propagating reaction fronts. The temporal evolution of the surface reaction results in a 'patterned' surface consisting of separated Au-rich and Au-poor phases with different oxygen coverage, Rh surface structure, and reactivity. The experimental results are complemented by ab initio electronic-structure calculations of the O and Au adsorption phases, which demonstrate that the reorganization of the Au adlayer by the propagating reaction fronts is an energetically driven process. Our findings suggest that reaction-induced spatial inhomogeneity in the surface composition and structure is a common feature of metal catalysts modified with adatoms which become mobile under reaction conditions.

1. Introduction

The composition and structure of metal catalyst surfaces evolves along well-known pathways governed by energetic principles.[1] Significant modifications can occur during reaction, because the adsorbed species affect the interface free energy and the mobility of the surface metal atoms.[2] Studies of spatio-temporal oscillations on transition metal catalysts indicate that also the adlayer composition is affected by the reaction, showing a variety of dissipative patterns and self-organization processes.[3−7] As has been reported recently, the mobile alkali adatoms, often used as modifiers, actively participate to the reaction-driven surface reorganization. The studies of the $O_2 + H_2$ and NO + H_2 reactions on Rh(110) model catalysts, modified with K or Cs, evidenced a reaction-induced generation of stationary concentration K (Cs) micro-patterns.[8−12] The key factor driving this reorganization process is the strong affinity of the mobile alkali adatoms to oxygen.[13] The attractive K(Cs)−O interactions destroy the lateral homogeneity of the surface, leading to the formation of two-dimensional islands consisting of dense and dilute K + O phases.

Surface reorganization processes involving mass transport are clearly interconnected to the adsorbate−adsorbate and adsorbate−substrate interactions. Such energetic drive implies that the reaction-driven mass transport of metal adatoms may occur for a broad class of catalytic systems. Here, we consider the water formation reaction in order to investigate whether the propagation of reduction/oxidation fronts induces compositional changes of the Rh(110) surface, modified with a Au adlayer. Under stationary reaction conditions, the water formation reaction on the Rh(110) surface is bi-stable, with the transition from an 'inactive' O-covered Rh surface to an 'active' O and H−free surface (and vice-versa) occurring with the propagation of elliptical reaction fronts.[14,15] The O-covered Rh(110) surface

† Sincrotrone Trieste S.C.p.A..
‡ Scuola Internazionale Superiore di Studi Avanzati and INFM DEMOCRITOS National Simulation Center.
§ Dipartimento di Fisica 'G.Galilei', Università di Padova.
|| Laboratorio Nazionale TASC.

(1) Venables, J. A.; Spiller, G. D. T.; Hanbucken, M. *Rep. Prog. Phys.* **1984**, *47*, 399.
(2) Chen, Q.; Richardson, N. V. *Prog. Surf. Sci.* **2003**, *73*, 59.
(3) Imbihl, R.; Ertl, G. *Chem. Rev.* **1995**, *95*, 697, and references therein.
(4) Ertl, G. *Science* **1991**, *254*, 1756.
(5) Zhdanov, V. P.; Kasemo, B. *Phys. Rev. B* **2000**, *62*, R4849−R4852.
(6) Zhdanov, V. P.; Kasemo, B. *Surf. Sci.* **2002**, *496*, 251.
(7) Sachs, C.; Hildebrand, M.; Völkening, S.; Wintterlin, J.; Ertl, G. *Science* **2001**, *293*, 1635.
(8) Günther, S.; Marbach, H.; Hoyer, R.; Imbihl, R.; Gregoratti, L.; Kiskinova, M. *J. Electron Spectrosc. Relat. Phenom.* **2001**, *114*, 989.
(9) Günther, S.; Marbach, H.; Hoyer, R.; Imbihl, R.; Gregoratti, L.; Barinov, A.; Kiskinova, M. *J. Chem. Phys.* **2002**, *117*, 2923.
(10) Marbach, H.; Günther, S.; Luerssen, B.; Gregoratti, L.; Kiskinova, M.; Imbihl, R. *Catal. Lett.* **2002**, *83*, 161.
(11) Marbach, H.; Lilienkamp, G.; Han, W.; Günther, S.; Suchorski, Y.; Imbihl, R. *Phys. Chem. Chem. Phys.* **2003**, *5*, 2730.
(12) Lilienkamp, G.; Han, W; Maus-Friedrichs, W.; Kempter, V.; Marbach, H.; Günther, S.; Suchorski, Y. *Surf. Sci.* **2003**, *532*, 132.
(13) De Decker, Y.; Marbach, H.; Hinz, M.; Günther S.; Kiskinova, M.; Michailov, A. S.; Imbihl, R. *Phys. Rev. Lett.* **2004**, *92*, 198305.
(14) Mertens, A.; Imbihl, R. *Chem. Phys. Lett.* **1995**, *242*, 211.
(15) Makeev, A.; Imbihl, R. *J. Chem. Phys.* **2000**, *113*, 3854.

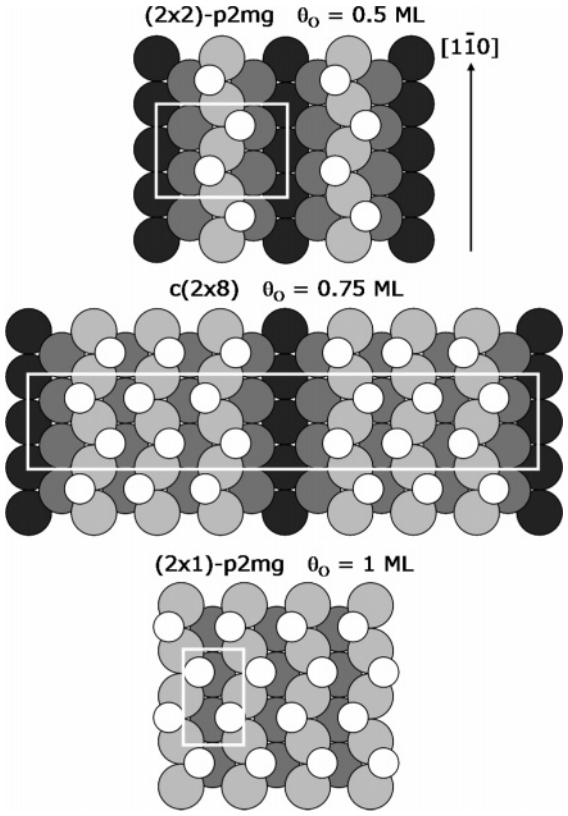

Figure 1. Hard sphere models of some O adsorption phases: (TOP) (1 × 2) reconstructed substrate with $\Theta_O = 0.5$ ML, which shows a (2 × 2)-p2mg LEED pattern; (MIDDLE) (1 × 4) reconstructed substrate with $\Theta_O = 0.75$ ML, which shows a c(2 × 8) LEED pattern; (BOTTOM) (1 × 1) unreconstructed surface with $\Theta_O = 1$ ML, which shows a (2 × 1)-p2mg LEED pattern.

shows a wealth of O-induced 'missing row' reconstructions with a zigzag arrangement of oxygen atoms in the 3-fold sites along the [110] rows, which can be lifted by reduction with H_2 or CO.[16] For clarity, the O-induced structures relevant to the present study are illustrated in Figure 1.

For the chosen reaction system, Au adatoms behave as inactive species, exerting a simple site-blocking effect due to a decrease of the number of available reaction sites.[17,18] According to the theoretical calculations, the Au adlayer on transition metal surfaces is less reactive than the surface of Au metal[19] and Au segregation on Rh is energetically favored with respect to the formation of a surface alloy.[20] Thus, the presence of Au adatoms influences the efficiency, but not the mechanism of the water formation reaction, which proceeds via O_2 and H_2 dissociative adsorption. O and H adatoms promptly react forming water, which immediately desorbs. At reaction temperatures higher than 400 K, the lifetime of adsorbed H is negligible and O remains the only stable adsorbed species.[21,22]

2. Experimental Section

We employed microscopic methods combining structural and chemical sensitivity in order to follow in-situ the reaction dynamics and the related reorganization of the catalyst surface and the adlayer. All experiments were performed with the Spectroscopic PhotoEmission and Low Energy Electron Microscope (SPELEEM) at the synchrotron light source in Trieste, Italy.[23,24] Using the X-ray beam as a probe, this instrument works as X-ray photoemission electron microscope (XPEEM) and micro-spot X-ray photoelectron spectroscope (μ-XPS). Using electron beam, it can be operated as LEEM and micro-spot low energy electron diffraction (μ-LEED), providing structural information at nano and micrometer scales.

LEEM imaging provides structural information with higher temporal and lateral resolution compared to XPEEM imaging.[25] Thus, it was extensively used to follow the dynamics of the propagating reaction fronts. Selecting an electron energy of ~8 eV maximized the Au backscattering and also enabled to distinguish between the O-covered (1 × *n*) reconstructed and O-free (1 × 1) Rh(110) surfaces. Under this condition, the LEEM and XPEEM Au 4f images show a remarkably similar contrast. However, the XPEEM imaging and μ-XPS were indispensable tools for quantification of the local surface composition.

The SPELEEM chamber was used as a gas flow reactor, where high purity H_2 and O_2 gases were introduced by means of precision leak valves. The sample temperature was measured with a WRe5%/WRe26% thermocouple. The reaction experiments were carried out in the temperature range 600−720 K, starting from two different surfaces, which we call Au-modified 'reduced' and Au-modified 'oxidized'. The 'reduced' and 'oxidized' surfaces were prepared in-situ, by depositing up to 0.8 ML[26] of Au at 600 K on an atomically clean Rh(110)−(1 × 1) surface or a Rh(110)−(1 × 4) surface covered with 0.75 ML of O (see Figure 1). A brief description of the Au adlayers growth on clean and 'oxidized' Rh(110) surfaces is given in the Supporting Information. To rule out possible effects of surface roughening and Au incorporation, resulting from the reconstruction−dereconstruction events induced by the propagating reaction fronts, we cleaned the Rh substrate and prepared a fresh Au-modified surface for each reaction cycle. Since the SPELEEM microscope operates in high vacuum, the O_2 and H_2 pressure was kept in the mid 10^{-7} mbar range. By varying the reactants' partial pressure, we were able to control with high precision the velocity and direction of the reaction fronts.

3. Results

3.1. Propagation of Reaction Fronts and Stationary State of the Reaction. The LEEM images in Figure 2A illustrate the ignition and propagation of reduction (RED) and consecutive concentric reoxidation (REOX) fronts, starting from a Au-

(16) Comelli, G.; Dhanak, V. R.; Kiskinova, M.; Prince K. C.; Rosei, R. *Surf. Sci. Rep.* **1998**, *32*, 165, and references therein.
(17) Rotermund, H. H.; Asakura, K.; Lauterbach, J.; Ertl, G. *Surf. Sci.* **1998**, *374*, 125.
(18) Besenbacher, B.; Chorkendorff, I.; Clausen, B. S.; Hammer, B.; Molenbroek, A. M.; Nørskov, J. K.; Stensgaard, I. *Science* **1998**, *279*, 1913.
(19) Hammer, B.; Nørskov, J. K. In *Impact of Surface Science on Catalysis*; Gates, B. C., Knözinger, H., Eds.; Academic Press: 2000; p 71.
(20) Christensen, A.; Ruban, A. V.; Stotze, P.; Jacobsen, K. W.; Skriver, H. L.; Nørskov, J. K.; Besenbacher, F. *Phys. Rev. B* **1997**, *56*, 5822.
(21) Norton, P. R. In. *The Chemical Physics of Solid Surfaces and Heterogeneous Catalysis*; Elsevier: Amsterdam, 1982; Vol. 4, 27.
(22) Fassihi, M.; Zhadanov, V. P.; Rinnemo, M.; Keck, K.-E.; Kasemo, B. *J. Catal.* **1993**, *141*, 438.
(23) Schmidt, Th.; Heun, S.; Slezak, J.; Diaz, J.; Prince, K. C.; Lilienkamp, G.; Bauer, E. *Surf. Rev. Lett.* **1998**, *5*, 1287.
(24) Locatelli, A.; Bianco, A.; Cocco, D.; Cherifi, S.; Heun S.; Marsi, M.; Pasqualetto, M.; Bauer, E. *J. Phys. IV* **2003**, *104*, 99; http://www.elettra.trieste.it/experiments/beamlines/nano/index.html.
(25) The SPELEEM can perform chemical imaging in XPEEM mode with a temporal resolution of 5 s, lateral resolution ≥30 nm and energy resolution ≥0.3 eV. In LEEM operation, it achieves a temporal resolution of 10 ms and a lateral resolution 10 nm. μ-XPS is measured with an energy resolution of 0.25 eV. μ-XPS and μ-LEED probe an area of ~4 μm^2.
(26) We define the monolayer ML as the number of atoms of the first layer of the Rh(110)−(1 × 1) surface.

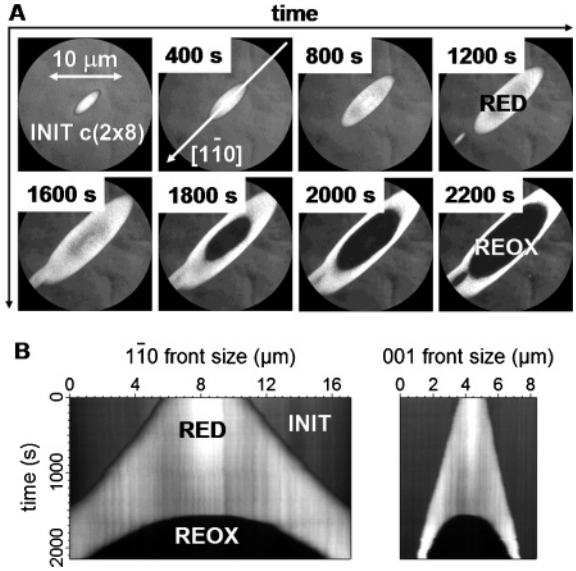

Figure 2. (A) LEEM images illustrating the ignition and propagation of a reduction front (RED) on 'oxidized' Rh(110) surface with 0.5 ML of Au (INIT), followed by a consecutive reoxidation (REOX) front. (B) Intensity profiles across the reaction fronts along the [1$\bar{1}$0] and [001] axes vs reaction time, measured from sequential LEEM images. Reaction parameters: $P[O_2] = 4.4 \times 10^{-7}$ mbar, $P[H_2] = 3.8 \times 10^{-7}$ mbar, $T = 720$ K.

modified 'oxidized' surface (INIT). The dynamics of the propagating 'RED' and 'REOX' fronts is described by the temporal evolution of the LEEM intensity profiles of the two fronts, taken along the main crystallographic axes (Figure 2B). It is evident that, after ignition, the REOX front velocity decreases and equalizes with that of the RED front. Similar reduction/reoxidation fronts were reproduced for the same partial pressure of the reactants, at temperatures from 600 to 720 K. The measured front velocities were in the range of a few nm/s, at least an order of magnitude lower than those measured under similar reaction conditions on the Au-free Rh surface. The decreased front velocity can be attributed to the steric site-blocking effects exerted by Au adatoms on oxygen and hydrogen adsorption, as in the case of CO oxidation on Au-covered Pt.[17]

The effect of the front propagation on the Au lateral distribution was verified by XPEEM and μ-XPS, by imaging the Au 4f electron emission and measuring the Au 4f spectra in the different developed regions. The Au 4f images remained featureless until the ignition of reoxidation fronts, i.e., the reduction fronts do not affect the initially homogeneous Au distribution. The Au $4f_{7/2}$ image in Figure 3B shows a detail of the advanced stage of the reaction with fully developed reoxidations fronts. The Au 4f image contrast reflects the variations in the Au concentration across the reaction front: the bright areas are the reduced Au-enriched regions, which is in qualitative agreement with the corresponding LEEM image in Figure 3C. It is clear that the concentration of Au in the RED areas has increased at the expense of Au from the REOX regions, due to the Au mass transport triggered by the reoxidation fronts.

Keeping the reaction parameters constant, the reduction/reoxidation fronts continue their propagation until complete removal of O from the initial $c(2 \times 8)$−O phase (see Figure 3A). When the fronts collide, the shape of the reduced and reoxidized domains can change significantly until a stable lateral configuration is achieved. The LEEM, μ-LEED, and μ-XPS data

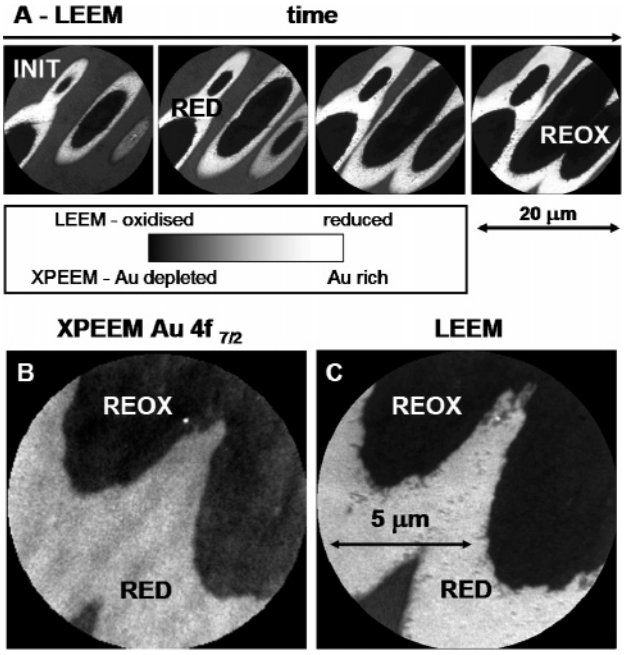

Figure 3. (A) LEEM images illustrating the evolution of the reaction fronts toward a stationary state. The developed reoxidation fronts (REOX) have triggered the redistribution of Au, which accumulates on the already reduced surface (RED), as confirmed by the Au $4f_{7/2}$ XPEEM image (B). (C) LEEM image corresponding to (B). Reaction parameters: $P[O_2] = 4.4 \times 10^{-7}$ mbar, $P[H_2] = 3.8 \times 10^{-7}$ mbar, $T = 620$ K.

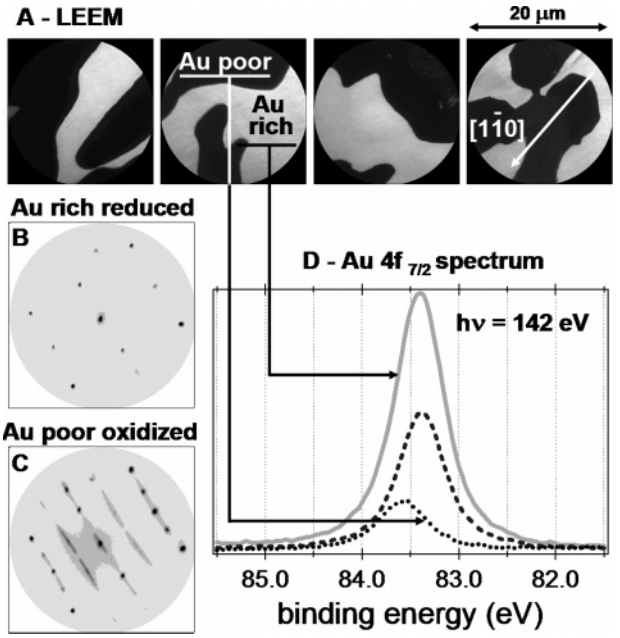

Figure 4. (A) LEEM images in different parts of the surface taken after establishment of the stationary state, where the Au-rich 'reduced' and Au-poor 'oxidized' phases appear bright and dark, respectively. (B, C) μ-LEED patterns of the Au-rich 'reduced' and Au-poor 'oxidized' phases; (D) μ-XPS Au 4f spectra of the Au-rich 'reduced' (full line) and Au-poor 'oxidized' (dotted line) phases. The dashed-line spectrum corresponds to the same Au adlayer homogeneously distributed on the reduced surface. Same reaction conditions as in Figure 3.

in Figure 4 show that the established stationary state consists of two coexisting phases. The first is a Rh(110)−(1×1) surface with high Au coverage, which we call Au-rich 'reduced' phase (the μ-XPS O 1s spectra confirmed the absence of O in these region). The second is a reconstructed Rh(110)−(1×2) surface with $\leq$0.5 ML of oxygen and low Au coverage, which we call

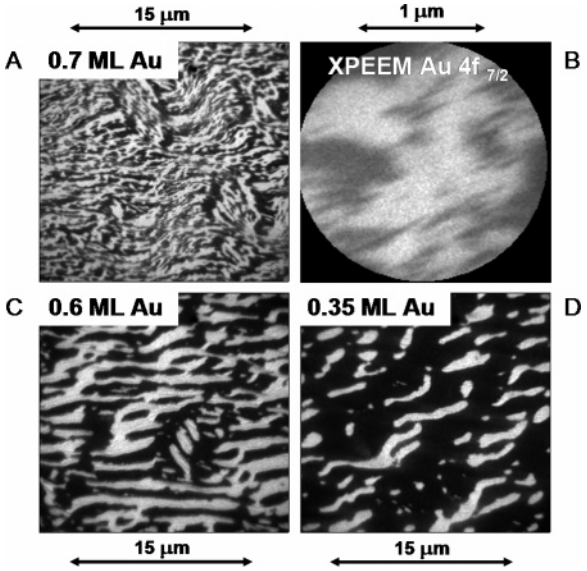

Figure 5. (A) LEEM image illustrating the prompt phase separation (bright-'reduced' and dark-'oxidized'), induced by the oxidation fronts ignited on a Rh(110)−(1 × 1) surface with 0.7 ML Au. (B) XPEEM Au $4f_{7/2}$ image of a subset of (A), illustrating the redistribution of Au coverage between the developed phases. (C,D) LEEM images illustrating how the relative area of the Au-rich 'reduced' phase increases with increasing initial Au coverage. Reaction parameters: $P[O_2] = 4.2 \times 10^{-7}$ mbar, $P[H_2] = 3.0 \times 10^{-7}$ mbar, $T = 720$ K.

Au-poor 'oxidized' phase. The (2 × 2)-p2mg LEED pattern of the Au-poor 'oxidized' phase is 'streaky' along the [001] direction, indicating the lack of order in the oxygen adlayer. Simple calculations show that the local Au coverage in the reduced region approaches a monolayer,[26] whereas the Au coverage of the 'oxidized' phase has dropped to ∼0.2 ML. The Au 4f binding energy (BE) shift of 0.19 eV between the 'reduced' and the 'oxidized' phase reflects the different chemical and structural environment of the Au adatoms. The laterally averaged Au 4f intensity remains constant before and after pattern formation, which excludes any sensible subsurface Au migration, in accordance with the theoretical predictions.[20] The formation of a stationary state with coexisting 'oxidized' and the 'reduced' phases does not occur on the Au-free surface, where the front propagation always leads to complete reduction or oxidation of the surface.

The formation of Au concentration patterns was also observed starting with a Au-modified 'reduced' Rh(110)−(1 × 1) surface. In this case, the Au mass transport starts promptly with the ignition of oxidation fronts and the final stationary state consists of the same two phases described above. The LEEM image in Figure 5A illustrates how the oxidation fronts (dark), ignited at the step edges, tend to compress the Au adatoms toward the neighboring O-free atomic terraces (bright). The temporal evolution of the system is such that the bright domains coalesce into larger islands (see also the Synopsis TOC). The aggregation of Au into islands is clearly demonstrated by the XPEEM Au 4f image in Figure 5B. The Au mass transport leading to development of a Au-patterned surface was observed for a rather wide range of Au coverages (0.3−0.8 ML) and temperatures. The relative area of the Au-rich 'reduced' phase is proportional to the initial Au coverage (compare Figure 5, parts C and D). The exact local Au and O coverage in the Au-rich and Au-poor phases of the stationary stage can slightly vary by changing the reaction conditions, but the trend is always preserved.

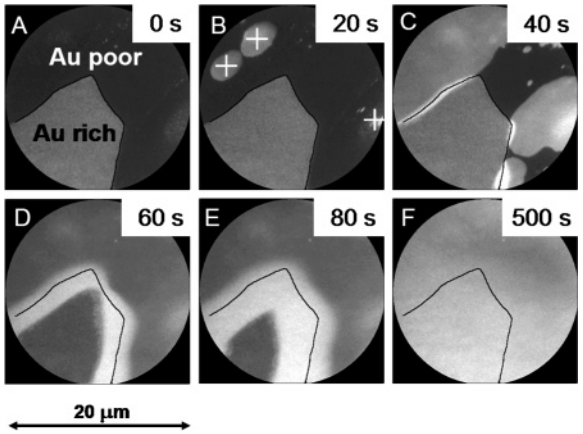

Figure 6. LEEM images illustrating the different activity of the oxygen-saturated Au-rich and Au-poor phases exposed to H_2 ambient. (A) initial state; (B) ignition of reduction fronts in the Au-poor region (+); (C) fast expansion of the reduction fronts, some of them reaching the Au-rich region; (D,E) slower propagation of the reduction fronts inside the Au-rich region, accompanied by Au redistribution; (F) completely reduced final state. Reaction conditions: $P[O_2] = 4.4 \times 10^{-7}$ mbar, $P[H_2] = 6.5 \times 10^{-7}$ mbar, $T = 620$ K. The black contour indicates the borders of the Au-rich phase before reduction.

3.2. Local Reactivity of the Au-Patterned Surface. The two phases observed at the stationary state exhibit different reactivity and can be viewed as independent microreactors. In O_2 ambient the two phases appear still reactive, but have different capacity for oxygen adsorption. The Au-rich 'reduced' (1 × 1) phase adsorbs limited amount of oxygen (≤0.5 ML) and undergoes a (1 × 2) reconstruction, whereas the Au-depleted 'oxidized' (1 × 2) phase adsorbs more oxygen (up to ∼0.75 ML) and undergoes a (1 × 4) deconstruction. Contrary to the case of the alkali-modified surface,[8−13] the Au pattern is preserved under oxidizing conditions. The oxygen-saturated phases of the Au-patterned surface also exhibit different local activity when exposed to H_2 ambient. The LEEM images in Figure 6 show how the reduction fronts are ignited only inside the Au-poor phase. The fronts progress quickly toward the periphery of the Au-rich phase and slow down when penetrating the latter. The subsequent reduction of the Au-rich phase is accompanied by a mass transport of Au toward the Au-poor areas, until homogenizing the Au coverage. The Au homogenizing process also occurs upon direct exposure of the stationary state to a H_2 ambient. The XPEEM images and the plot in Figure 7 illustrate how the Au adatoms from the Au-rich 'reduced' phase of the stationary state diffuse toward the Au-poor regions after removal of oxygen, accompanied by lifting of the (1 × 2) substrate reconstruction.

4. Discussion

The behavior of the Au/Rh system during the water formation reaction shows several analogies with the case of K/Rh system.[8−13] The most striking is the formation of a stationary pattern during the transition from reduction to oxidation conditions, as illustrated by the LEEM and XPEEM images in Figure 5, parts A and B, and in the synopsis TOC. The observed patterns are nonequilibrium structures, because they form and exist only under definite reaction conditions. The Au patterns are destroyed only under reduction, whereas the K patterns are also destroyed under oxidation. The length scale of the Au patterns depends on the reaction conditions: the Au coverage,

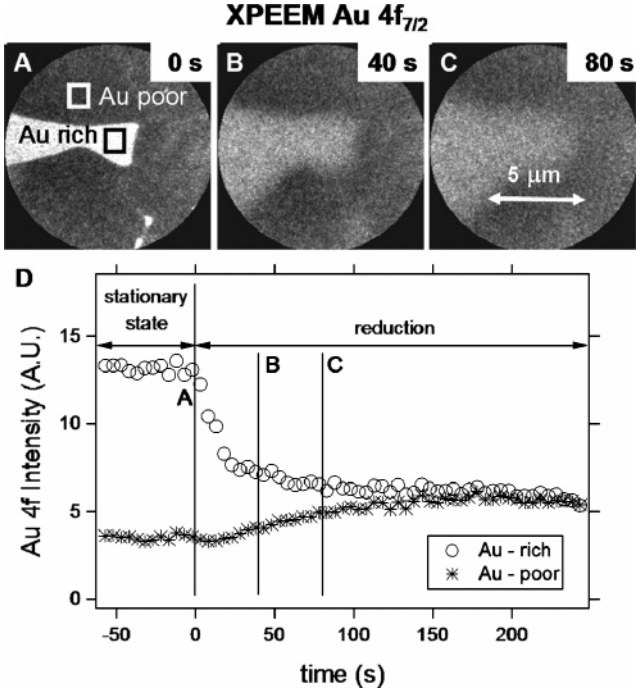

Figure 7. XPEEM Au $4f_{7/2}$ images illustrating homogenization of Au coverage by exposing of a stationary state to H_2 ambient. (A) initial state with Au-rich 'reduced' phase (bright) surrounded by a Au-poor 'oxidized' phase; (B,C) fast redistribution of Au coverage occurring while reacting the oxygen from the Au-poor phase. (D) Plot of the temporal evolution of the Au $4f_{7/2}$ intensity from the regions indicated by the squares in (A), illustrating the homogenization process. Reaction parameters: $P[O_2] = 4.4 \times 10^{-7}$ mbar, $P[H_2] = 6.5 \times 10^{-7}$ mbar, $T = 610$ K.

the reactants' pressure and sample temperature, as shown in Figure 5, parts C and D. The pattern is always formed during propagation of oxidation fronts under 'mild' oxidation conditions. We observed that a 'fast' transition from reduction to oxidation conditions produces nanoscopic patterns. On the other hand, a very 'slow' transition is responsible for the formation of a mesoscopic pattern. Finally, if the temperature is too low (less than 500 K), the reorganization cannot take place because the Au diffusion channel is not enabled. In analogy with the case of the K/Rh system, the formation of the Au stationary patterns may be attributed to a Turing-like instability of the uniform state.[13] However, the observed reorganization differs from that of the original Turing definition, which accounts only for the different diffusion rates of the reacting species.[27] Our experimental data indicate that the pattern formation is a reaction-driven process occurring at nanoscopic level, starting with the nucleation of oxygen islands, as shown in Figure 5A. As discussed below, the energetic difference between the possible adsorption phases plays a crucial role in the reaction-driven pattern formation.

The knowledge of the energetic of the system is of fundamental importance for the kinetic description of pattern formation. For example, the diffusion equations in ref 13 are applicable to a reacting system consisting of two reactants and a promoter/poison. They contain a term representing the 'viscous' flow of adsorbates, which includes the potential gradients of the attractive (repulsive) interaction between adsorbates. In complex reaction systems, such as Au/Rh, along with the adsorbate mutual interactions, it is essential to consider the adsorbate−substrate interactions. To quantify the driving force responsible for the formation of the Au concentration patterns, we complemented our experimental findings by ab initio electronic-structure calculations, elucidating the energetics of the O and Au adsorption phases.

Table 1. Binding Energies of Au on a Rh(110)−(1 × 1) Surface

Au coverage, Θ_{Au} (ML)	adsorption structure	binding energy (eV/atom)
0.25	(2 × 2) hollow	3.39
0.50	(1 × 2) hollow	3.61
0.50	(2 × 1) hollow	3.43
0.50	(2 × 2) hollow	3.39
0.75	(2 × 2) hollow	3.54
1.00	(1 × 1) hollow	3.59

Ab initio simulations were performed within density-functional theory (DFT) in the generalized gradient approximation of Perdew, Burke, and Ernzerhof (PBE).[28] We used ultrasoft pseudo-potentials[29] and plane-wave basis sets up to a kinetic-energy cutoff of 27 Ry (216 Ry for the density). Isolated surfaces were simulated with periodically repeated slabs of 6 Rh atomic layers, with the first two layers fixed at the bulk truncated structure and the others free to relax. The slabs were separated by a vacuum region of at least 8 Å. Brillouin-zone integrations were performed with the Gaussian-smearing special-point technique (3 × 4 × 2 BZ sampling).[30,31] We have estimated that the overall numerical accuracy in the binding energy due to all these approximations is of the order of 0.01 eV. All the calculations have been performed with the PWscf package.[32]

We start with discussing the adsorption of Au on the Rh(110)−(1 × 1) surface. Four different adsorption configurations were investigated, corresponding to 'on-top', 2-fold 'long bridge' and 'short bridge' and to the 4-fold 'hollow' sites. The calculations indicate that Au binds to the surface exclusively in the hollow site, the other configurations being unstable. In Table 1 we report the computed binding energies at different Au coverages ($\Theta_{Au} = 0.25$, 0.50, 0.75, and 1.00 ML). At the coverage of $\Theta_{Au} = 0.5$ ML the following three different adsorption structures (characterized by different periodicities) are possible: the (1 × 2) with Au atoms aligned along the $[1\bar{1}0]$ direction, the (2 × 1) with Au aligned along the [001] direction and the (2 × 2) with Au aligned along the $[1\bar{1}1]$ direction. The (1 × 2) configuration with Au chains along the $[1\bar{1}0]$ direction turned out to be the energetically favored one. The energy gain with respect to the 0.25 ML coverage is due to an increase of the attractive interaction between the Au adatoms, which is much stronger along the $[1\bar{1}0]$ direction, 0.11 eV/atom for a couple of Au atoms compared to 0.02 eV/atom along the [001] direction (the interaction along the $[1\bar{1}1]$ direction is negligible). These attractive interactions favor the formation of chains along the $[1\bar{1}0]$ direction at intermediate coverage, and a pseudomorphic monolayer at saturation. This implies that at low temperatures the Au adatoms will tend to cluster along the $[1\bar{1}0]$ direction even at low coverage. Our calculations also show that the

(27) *Chemical Waves and Patterns*; Kapral, R., Showalter, K., Eds.; Kluwer: Dordrecht, 1994.

(28) Perdew, J. P.; Burke, K.; Ernzerhof, M. *Phys. Rev. Lett.* **1996**, *77*, 3865.
(29) Vanderbilt, D. *Phys. Rev. B* **1990**, *41*, 7892.
(30) Monkhorst, H. J.; Pack, J. D. *Phys. Rev. B* **1976**, *13*, 5188.
(31) Methfessel, M.; Paxton, A. T. *Phys. Rev. B* **1989**, *40*, 3616.
(32) Baroni, S.; Dal Corso, A.; De Gironcoli, S.; Giannozzi, P.; http://www.pwscf.org.

Table 2. Binding Energies of Au on an O-Covered Rh(110) Surface

	$\Theta_O = 0.5$ ML	$\Theta_O = 1.0$ ML
$\Theta_{Au} = 0.25$ ML	2.93 eV/atom	1.36 eV/atom
$\Theta_{Au} = 0.50$ ML	3.08 eV/atom	2.08 eV/atom
$\Theta_{Au} = 1.00$ ML		2.26 eV/atom

binding energy of Au adatoms is not sensibly affected by the (1 × 2) reconstruction of the substrate. On the (1 × 2) reconstructed surface, where the first Au adlayer equals 0.5 ML, we found a binding energy of 3.38 eV/atom for $\Theta_{Au} = 0.25$ ML and 3.58 eV/atom for $\Theta_{Au} = 0.5$ ML. Again, there is a strong attractive interaction (0.10 eV/atom) along the [1$\bar{1}$0] direction.

A detailed ab initio description of the oxygen adsorption on the Au-free Rh(110) surface is presented in ref 33. For oxygen coverage of 0.5 ML on the (1 × 2) surface and of 1 ML on the (1 × 1) surface, O occupies the 3-fold fcc hollow sites, arranged along the (110) rows in a zigzag fashion (see Figure 1), in agreement with the experimental findings.[16] Our calculations confirm this picture, but correct the binding energies overestimated by the local density approximation (LDA) used in ref 33. We obtain a binding energy of 2.15 eV/atom for $\Theta_O = 0.5$ ML on the (1 × 2) surface (LDA value = 2.75 eV) and 1.67 eV/atom for $\Theta_O = 1$ ML on a (1 × 1) surface (LDA value = 2.23 eV). The (1 × *n*) reconstructed surfaces with Θ_O between 0.5 and 0.8 ML (i.e., $n > 2$), where O adatoms adsorbed along the (1 × 2) and (1 × 1) troughs coexist (see Figure 1), can be described referring to the O−(2 × 2)-p2mg and the O−(2 × 1)-p2mg adsorption configurations.

To explain the reorganization of Au adlayer during the water formation reaction, we calculated the Au binding energy in coadsorbed systems at low and high Au and O coverage (Table 2). We found that at $\Theta_O = 0.5$ ML on a (1 × 2) surface, Au preserves the 'hollow' adsorption site with attraction between the Au atoms along the [1$\bar{1}$0] direction, but its binding energy is reduced by 0.5 eV with respect to that on the clean (1 × 2) surface. The Au binding energy decreases considerably on an oxygen saturated (1 × 1) surface ($\Theta_O = 1$ ML). A notable feature is that in the coadsorbed systems the attractive interactions between Au atoms along the [1$\bar{1}$0] direction have increased to 0.36 eV/atom, compared with 0.11 eV/atom for the clean surface. This indicates that presence of oxygen favors the Au clustering along the [1$\bar{1}$0] direction.

To quantify the contribution of the overall energetic balance between coadsorbed Au and O we calculated the mixing energy, E_{mix}, defined as the difference in the total binding energy between the separate Au and O phases and the mixed (Au + O) phase. E_{mix} is normalized to the number of adsorbed Au and O atoms in the cell and represents the contribution of the overall attractive/repulsive interactions per atom. It is calculated using the relationship

$$E_{mix} = (E_{Au}[\Theta_{Au}] + E_O[\Theta_{Au}] - E_{Au+O}[\Theta_{Au+O}])/N$$

where Θ_{Au}, Θ_O are the Au and O coverages of the separate Au and O adsorption phases, and Θ_{Au+O} is the total Au + O coverage in the coadsorbed phase. As can be seen in Figure 8, E_{mix} is always positive and increases with increasing density of the coadsorbed phase, as a consequence of both the weakened bonding of Au on the O-covered Rh surface and steric hindrance effects. This result indicates that the separated Au and O phases are energetically more favorable than coadsorbed Au + O phase.

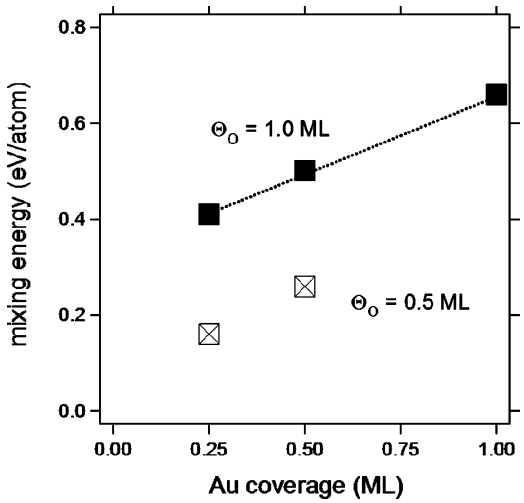

Figure 8. Mixing energy, E_{mix}, is plotted for increasing Au coverage, in the case of 0.5 ML (open squares) and 1.0 ML (full squares) oxygen coverage. The dashed line serves as a guide for the eye. Positive values of E_{mix} indicate that the coadsorbed phase is not energetically favorable.

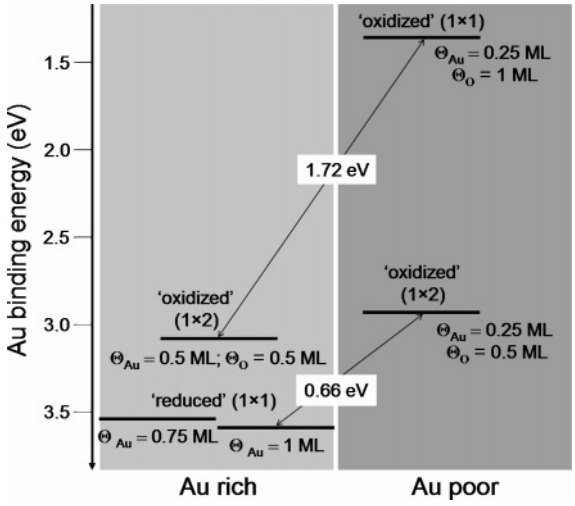

Figure 9. Energetics of Au adsorption in the Au rich and Au poor phases.

The energetic balance elucidated by the ab initio calculations provides an excellent explanation why the Au reorganization, ending with a stationary patterned surface, is triggered only by the oxidation fronts. This occurs because the Au adatoms are more strongly bound on the clean rather than on the 'oxidized' Rh surface (see Figure 9). Provided the mobility of the Au adatoms is high enough, they will tend to migrate and accumulate in the reduced surface, thus leaving behind O-covered Au-poor regions, as clearly illustrated in Figure 5. In fact, the oxidation front acts like a 'moving' potential energy barrier that compresses gold atoms toward the energetically favored reduced (1 × 1) surface until the saturation monolayer Au coverage is achieved.

It is obvious that, if we start with an 'oxidized' surface, homogeneously covered with Au, and ignite reduction fronts, their propagation will only remove the coadsorbed oxygen, thus strengthening the adsorption bond of Au. Only the subsequent reoxidation fronts will activate the Au reorganization. The direction of the reduction/reoxidation fronts is dictated by the

(33) Stokbro, K.; Baroni, S. *Surf. Sci.* **1997**, *370*, 166.

minimization of the free energy. For fixed reaction parameters, the energetic barriers for the diffusion of adsorbed atoms are only responsible of the velocity of the reaction fronts, but do not influence the stationary state, which is always characterized by the Au rich 'reduced' and Au poor 'oxidized' phases.

Also the stability of the patterned Au surface in O_2 ambient can be explained in terms of energetic considerations. As the Au binding energy decreases with increasing O coverage, the migration of Au adatoms from the Au-rich phase toward the Au-poor phase, which has higher oxygen coverage, is energetically unfavorable.

5. Conclusions

We demonstrate that in realistic catalytic systems involving modifying additives, complex 'patterned' interfaces can develop during surface reactions, even when the modifiers are chemically inert with respect to the reactants and exert only site-blocking effect. The present investigations confirm that the lateral reorganization of the adsorbed phases and the formation of stationary structures are not isolated cases, but universal phenomena in multicomponent catalytic systems. Provided the surface mobility of the adsorbed species is high enough, our analysis demonstrated that the reaction-induced reorganization of adsorbed layers on modified catalytic surfaces can be predicted and understood by exploiting the energetics of the possible adsorption phases.

Acknowledgment. The authors gratefully acknowledge the technical assistance of Michele Pasqualetto.

Supporting Information Available: A description of the growth and characterization of ultrathin Au films on Rh(110). This material is available free of charge via the Internet at http://pubs.acs.org.

JA045285K